Telluric field variations as drivers of variations in cathodic protection potential on a natural gas pipeline in New Zealand

M. Ingham[1] and C.J. Rodger[2]

[1] School of Chemical and Physical Sciences, Victoria University of Wellington, Wellington, New Zealand.
[2] Department of Physics, University of Otago, Dunedin, New Zealand.

Corresponding author: M. Ingham (malcolm.ingham@vuw.ac.nz)

Key Points:

- The cathodic protection potential on a New Zealand gas pipeline is found to vary significantly during a magnetic storm
- Contrary to simple theory, in this region the variations are found to be related to changes in the induced telluric field perpendicular to the pipeline
- This is a result of the electrical conductivity structure of the Earth associated with the tectonic setting of New Zealand

Abstract

A study of variations in cathodic protection potential on a natural gas pipeline in the North Island of New Zealand is reported. Both the measured pipe to soil potential (PSP) and the current measured through an installed defect in the pipeline coating show strong correlations with variations in measured magnetic and telluric fields. Contrary to predictions from distributed-source transmission line theory, analysis shows that the closest correlations of PSP and current are with the component of telluric field perpendicular to the pipeline. This orientation is close to perpendicular to major electrical conductivity contrasts associated with both the local coastline and with on-shore Earth conductivity structure. It is therefore inferred the variations in PSP which drive the variations in defect current are the result of changes in the local earth potential. While reporting on specific observations from New Zealand, these results should be applicable across a wide range of mid- and high-latitude global locations. Estimates of possible corrosion rates for the pipeline in question suggest that such enhancement of telluric field variations by conductivity structure may pose significant risk to pipelines in the event of defects in the pipeline coating.

Plain Language Summary

Temporal variations in Earth’s magnetic field induce electric fields in the ground. Rapid and large changes in the magnetic field, such as during magnetic storms, can produce earth currents that can have a significant impact on technological systems such as power transmission lines and oil and gas pipelines. Pipelines generally have an insulating coating. Should a break in this occur, electrochemical reactions can allow a current to pass from the pipe to the ground resulting in corrosion of the pipe. To further protect them pipelines generally have a voltage applied to them (cathodic protection) so that they are at a negative potential relative to the ground. In this study on a gas pipeline in New Zealand we found that during a magnetic storm the changes in the ground potential due to the variations in the magnetic field were often large enough to over-ride the cathodic protection so that the pipeline became positive relative to the ground. The orientation of the electric field that caused this does not agree with that expected from theory. This is due to the tectonic and geological structure of the area, and illustrates that the risk presented to cathodic protection systems may be more severe than previously thought.

1 Introduction

In recent years the risk posed to electrical power networks by space weather has been extensively studied in many parts of the world (e.g. Beggan et al., 2013; Blake et al., 2016; Bonner & Schultz, 2017; Divett et al., 2017; Gaunt & Coetzee, 2007; Ingham et al., 2017; Liu et al., 2009; Marshall et al., 2013; Torta et al., 2012, 2014, 2017; Trivedi et al., 2007). As recently reiterated by Boteler and Pirjola (2017), such risk arises from geomagnetically induced currents (GIC) driven by the electromotive force induced in long transmission lines. This force arises from variations in the magnetic field cutting a loop consisting of the line itself, the grounding points of the line, and a depth in the earth related to the skin-depth for the magnetic field variation. Modeling of the induced electric fields and their impact on a specific transmission line topology allows prediction of the severity of the risk presented by GIC to electrical substations, or even individual transformers, in the network (see for example, Divett et al., 2018).

Somewhat less well studied is the risk that space weather and GIC present to long pipelines, typically those carrying petroleum fuels or gas. Early work on this was presented by Gideon (1971) and by Campbell (1978, 1980) in relation to an Alaska pipeline. Subsequent studies have been related to GIC in Canadian and Finnish pipelines (Viljanen, 1989; Pulkkinen et al., 2001a; Viljanen et al., 2006; Fernberg et al., 2007), although such effects have also been observed in Argentina (Osella et al. 1998) and Australia (Marshall et al., 2010). Typically, pipelines are protected from corrosion by cathodic protection in which, in general, voltage sources placed along the pipeline keep the pipe potential negative with respect to the ground. If the pipeline potential is at least 0.85 V below that of ground then breaks in the pipeline coating will not cause corrosion as current will pass from ground to pipe rather than from pipe to ground. The risk to pipelines from space weather arises because GIC can result in such cathodic protection being over-ridden and the pipe to soil potential (PSP) becoming positive. The GIC and the associated pipe to soil potentials have generally been modeled by using distributed-source transmission line (DSTL) theory (e.g. Boteler, 2000; Pulkkinen et al., 2001b), although Boteler (2013) has suggested modeling induction in a pipeline using a nodal admittance network.

Within New Zealand GIC, and their effect on the power network, is an area of recent on-going research (e.g., Divett et al., 2017; Ingham et al., 2017; Mac Manus et al., 2017; Rodger et al., 2017), but there has been little focus to date on the effects on pipelines. However, on 14 September 2017 a pipeline (Figure 1(a)) carrying aviation fuel to Auckland International Airport failed causing major disruption to air travel (see for example, *https://www.stuff.co.nz/business/97019369/*). Although the ultimate cause of the failure is believed to have been damage caused by a mechanical digger some years previously which damaged the insulating coating and scraped the pipe itself, it is also pertinent to question whether or not space weather effects contributed to subsequent corrosion. This may be particularly relevant as the pipeline failure followed only 6 days after a geomagnetic storm during which the Kp-index reached a maximum of 8+, the implication being that the effect of this storm was such that the on-going corrosion of the pipeline since the original damage reached the point where the pipe failed.

In this paper we revisit an earlier, 1992, study, previously only published as a contract report (Ingham, 1993) but for which the original digital data, and fieldwork and analysis notes remain extant, of the effect of GIC on a pipeline close to the town of Dannevirke in the North Island of New Zealand. In this study PSP was measured in association with variations in the geomagnetic field, telluric (Earth electric) fields, and the current between ground and the pipeline through an installed artificial defect in the pipeline coating. At the time there was no generalized theory for calculating GIC in pipelines, and the conclusion was that the observed variations in PSP were largely the result of variations in the induced telluric field perpendicular to the pipeline. The original report noted that modeling showed that induced electric fields in the

North Island of New Zealand were largest around and to the north of Auckland (*Chen et al.*, 1990), the region in which the 2017 pipeline failure occurred. This region was consequently deemed to be at very high risk of corrosion in the event of a break in pipeline insulation. As noted above, there has been considerable subsequent development in the theory behind GIC in pipelines. Therefore, in this paper after describing the location of, and measurements that were made in the 1992 study, we present the main features of the original analysis and interpretation, and then discuss these in the light of the subsequent advances that have been made in understanding the effects of space weather on pipelines. We believe there have been relatively few such detailed observations of GIC in pipelines to date, and suggest this work should be a useful addition to the international literature.

2 1992 Study Location and Measurements

The location of the study on the natural gas pipeline at Dannevirke is shown in Figure 1(a). This pipeline, which is buried for its entire ~200 km length, provides the supply route for natural gas to the Hawkes Bay region on the east coast of the North Island of New Zealand. The study was conducted for the then National Gas Corporation of New Zealand Ltd. with three aims: (i) to confirm that observed variations in cathodic protection (CP) potential were geomagnetically driven; (ii) to attempt to deduce the actual mechanism producing these variations; and (iii) to quantify the likelihood of actual corrosion of the pipe in the event of a break in insulation. At the study location (Figure 1(b)) the declination (angle between geographic and magnetic north) was 21°E at the time of measurements and the local orientation of the pipeline was 39°E, approximately parallel to the main tectonic strike of New Zealand (see, for example, Beanland and Haines (1998)).

Over the period 28 February – 16 April 1992 the following measurements were made with a sampling interval of 60 seconds:

- 3 components of the magnetic field (magnetic north – *H*; magnetic east – *D*; vertical – *Z*)
- The telluric fields parallel (*N*) and perpendicular (*E*) to the pipeline.
- The cathodic protection potential (*PSP*) at a point along the pipe. Nominally this is set so that the pipe is at -1100 mV relative to ground.
- The current (*I*) through a 1 Ω resistor in series with a specifically installed metal coupon connecting the pipe to the ground about 100 m south-west of the *PSP* measurement location. A positive value of *I* represents a current from ground to pipe.
- The along pipe potential difference (V_P) over a distance of 20 m just to the south of the location of the measurement of *PSP*. A positive value of V_P represents a current in the pipe from south-west to north-east.

Measurement of V_P, given the quoted pipe resistance of 22.9 μΩ/m, allows calculation of the along pipe current (I_P) with the current in mA related to V_P in mV by

$$I_P = 2183.4\, V_P \tag{1}$$

This measurement of along pipe current differs significantly from the method used, for example, by Pulkkinen et al. (2001a) who measured the magnetic field variations directly above a pipeline and, after subtraction of the field measured at a nearby geomagnetic observatory, used Ampere's Law to calculate the current.

Over the measurement period there was substantial magnetic activity which resulted in significant variations in cathodic protection potential, along pipe potential difference, and the coupon current. At times of high activity large variations were observed in all the measured parameters. In particular, a magnetic storm of significant duration commenced at approximately 2200 local time on 29 February (i.e. ~0900 UT) 1992. The effects resulting from this storm are representative of the whole measurement period. Shown in Figure 2 are the measured variations in the parameters *H*, *D*, *N*, *E*, *PSP*, *I* and V_P for the subsequent magnetically active day of 1 March 1992 local time. This period of 24 hours corresponds to the main phase of the storm. The main features that are apparent in Figure 2 and in measurements from other days in the recording period were summarized by Ingham (1993) as follows.

- A visually strong correlation exists between variations in the magnetic field and all of the other measured parameters. This is most clearly apparent in the high frequency variations associated with the magnetic storm (Figure 2), although very low frequency variations in the magnetic field (e.g., the daily variation) also correlate with variations in *N*, *E*, *PSP* and *I*. On magnetically quieter days the amplitudes of the higher frequency variations are considerably smaller yet still induce visible and correlated variations in the other parameters.
- Calculated correlation coefficients between *PSP* and *H* (-0.469) and *D* (-0.241) reflect the fact that, notwithstanding the visual similarity, phase differences exist between variations in the different parameters.
- The variations in the telluric field perpendicular to the pipe (*E*) are significantly larger than those parallel to the pipe (*N*).
- During periods of intense magnetic activity (e.g. 0500-1000 local time in Figure 2) *PSP* becomes positive i.e. the pipe becomes positive with respect to ground, overcoming the cathodic protection system. At these times, as expected the ground to pipe current (*I*) becomes negative – current passes from pipe to ground.
- *I* also (just) becomes negative on two occasions in Figure 2 (approximately 0130 and 1930 local time) when *PSP* exhibits large excursions but does not actually become positive. This is probably a reflection of slight variations in the cathodic protection potential along the pipe.

On 1 March V_P varies between -0.5 mV and about +0.8 mV indicating a current along the pipeline of about 1 A maximum which alternates in direction in response to changes in the along pipe potential difference – a positive value of V_P indicating a current directed to the north-east. Using Ampere's Law and a distance of ~20 m between pipe and the magnetometer, this implies a maximum contribution to the total measured magnetic field of about 5 nT. The orientation of this contribution is principally in the vertical and magnetic east directions.

3 Analysis

Ingham (1993) presented a detailed analysis of the observations and drew several conclusions as to the origin of the variations in cathodic protection potential and the ground to pipe current through the installed defect. Although the following discussion largely follows this analysis it is phrased in the context of how well the measurements can be explained in terms of the subsequent development of understanding into the origin and impact of GIC on pipelines over the last 25 years. As the potential impact on a pipeline largely relates to the over-riding of the cathodic protection system and the resulting possibility of corrosion, much of the analysis centres on variations in the ground to pipe current (I) as measured through the artificial defect.

3.1. Variation of *I* with rates of change of the horizontal magnetic field

Both intuitively, and as deduced from DSTL theory, GIC in a pipeline can be expected to be driven by the rate of change of the horizontal magnetic field perpendicular to the pipeline (e.g. Pulkkinen et al., 2001b). Although measurements of the magnetic field were made in geomagnetic coordinates, knowledge of the declination and the orientation of the pipeline means that these can easily be rotated into values parallel (H_{par}) and perpendicular (H_{perp}) to the pipeline. From these the time derivatives of the field in nT/min can be derived. Shown in Figure 3 for the period 0700-1100 local time on 1 March 1992 are plots of these derivatives and also of measured values of the ground to pipe current (I). Highlighted by the vertical dashed lines are instances where I (upper panel) becomes negative – that is, times when the cathodic protection system is over-ridden and current passes from pipe to ground – times when any defect in the pipeline coating would lead to corrosion.

The major occurrences of this shown in Figure 3 are between 8.5 and 9.5 hours, local time. All of these occur at times when the rate of change of the field parallel to the pipeline (middle panel) is at, or very close to, a negative peak. However, even with the limited time resolution, the same is not true for dH_{perp}/dt (lower panel). Indeed the second, third and fifth occurrences of pipe to ground current occur at times when this rate of change is very close to zero.

Observations such as this, suggest that variations in the field parallel to the pipeline play a significant role in causing variations in *PSP* and I.   This led to the inference in Ingham (1993) that "*…the processes involved in inducing changes in cathodic protection potential are more complex than simple theory would predict…*".

3.2. Transfer function analysis

Following analysis of how pipe to ground current correlated with rates of change of the magnetic field, Ingham (1993) discussed the calculation of frequency dependent transfer functions between variations in I and in the measured horizontal components of the magnetic field. As outlined by Ingham et al. (2017) this requires Fourier Transformation of simultaneous time series of I and the measured magnetic field variations, and calculation from these of autopower and cross-power spectra. Transfer functions in the period range 2 minutes to slightly less than 100 minutes were calculated by Ingham (1993) using multiple 6 hour data sections from the period 29 February to 5 March 1992 such that:

$$I(f) = A(f)H(f) + B(f)D(f) \qquad (2)$$

in which *A* and *B* are complex quantities, the ratio of imaginary to real parts being related to the phase of the current variations relative to the magnetic field variations.

Although the original transfer functions were calculated in geomagnetic coordinates, it is convenient to rotate these into an axial system where variations in *I* are related to those in the magnetic fields parallel (H_{par}) and perpendicular to the pipeline (H_{perp}). In this system

$$I(f) = R(f)H_{par}(f) + S(f)H_{perp}(f) \qquad (3)$$

where

$$R(f) = A(f)\cos\alpha + B(f)\sin\alpha$$

$$S(f) = -A(f)\sin\alpha + B(f)\cos\alpha$$

α being the clockwise angle (18°) between magnetic north and the orientation of the pipeline. Plots of *R* and *S* as a function of period, calculated using approximately 16 hour data sections, giving transfer functions to longer periods than the original calculation, are shown in Figure 4. Uncertainties and scatter in *S* are considerably larger than in *R*. Nonetheless, at all except the shortest and longest periods of variation the magnitudes of both the in-phase (real) and quadrature-phase (imaginary) parts of *R* are at least as large, if not larger, than those of *S*. This led Ingham (1993) to the conclusion that variations in *I* are driven at least as much by variations in H_{par} as by variations in the component of the field perpendicular to the pipeline (H_{perp}). The fact that the real and quadrature parts of *R*, in particular, are comparable in magnitude suggested that *I* is responsive to both H_{par} and its rate of change. The main peak in response is approximately in the period range 6 – 30 minutes.

It is useful to calculate the orientation of variations in the magnetic field which lead to maximum variation in the ground to pipe current at each period. Although this does not necessarily indicate the specific orientation of field variations which are responsible for causing changes in *I*, it does indicate the sensitivity of *I* to orientation of the field variations. For example, in studies of geomagnetic induction in the Earth it is common to relate observed variations in the vertical component of the field (*Z*) to those in the horizontal field by calculating so-called induction arrows. Thus when variations in *Z* are related to those in *H* and *D* by transfer functions *A* and *B*, in-phase (real) and quadrature-phase (imaginary) induction arrows are defined, at some period *T*, by

$$|Real| = (A_r^2 + B_r^2)^{1/2} \qquad \tan\theta_{Real} = B_r / A_r \qquad (4a)$$

$$|Quad| = (A_i^2 + B_i^2)^{1/2} \qquad \tan\theta_{Imag} = B_i / A_i \qquad (4b)$$

where A_r, B_r are the real parts of A and B, and A_i, B_i the imaginary parts. The directions of the arrows indicate the orientation of horizontal field variations to which the vertical field changes have maximum correlation. The magnitudes, or lengths, of the arrows indicate the relative magnitudes of the variations in the vertical field to those in the horizontal field in this orientation (Ritter, 2007).

As an alternative, for a unit magnetic field variation at an angle θ clockwise from the pipeline orientation, the amplitudes of variations in H_{par} and H_{perp} are $\cos(\theta)$ and $\sin(\theta)$ respectively. The resulting frequency dependent variation in I is therefore

$$I(f) = R(f)\cos\theta + S(f)\sin\theta$$

Multiplying this equation by its complex conjugate and differentiating with respect to θ allows the field orientation which produces maximum overall variation in I to be determined as the solution of

$$\tan 2\theta = \frac{2(R_r S_r + R_i S_i)}{({R_r}^2 + {R_i}^2 - {S_r}^2 - {S_i}^2)} \qquad (5)$$

The results of calculation of θ using (5) are shown in Table 1, including the calculated uncertainties in the angle based on those in the transfer functions. Calculations of both θ_{Real} and θ_{Imag} using equations (4) give essentially the same angles for periods greater than about 50 minutes. At shorter periods θ_{Real} and θ_{Imag} differ and not only does the angle θ shown in Table 1 correspond to an approximate average of these, but there is also a resulting larger uncertainty.

The results appear to suggest that there is a difference in response to the horizontal magnetic field orientation between shorter and longer periods of variation. However, for periods of variation up to about 8 minutes the large uncertainties in angle result from the fact that the magnitude of current is actually insensitive to the orientation of the magnetic field changes, meaning that a preferred orientation is very poorly defined. It is only for periods of 50 minutes or above that the magnitude of the current variation falls off rapidly as the field orientation moves away from that shown in Table 1. At these periods θ is relatively close to the local direction of magnetic north. What is clear is that at no period does the ground to pipe current appear to be most responsive to variations in the magnetic field component perpendicular to the pipeline. The periods of variation which cause the largest amplitude fluctuations in ground to pipe current are confirmed as those in the range of approximately 6 – 30 minutes.

Transfer functions (U and V) can similarly be calculated between I and the measured electric fields (E_{par} and E_{perp}) parallel and perpendicular to the pipeline. These transfer functions are shown in Figure 5. Whereas both in-phase (real) and quadrature-phase (imaginary) parts of V are very well estimated and show a smooth variation with period, the real and imaginary parts of U are both more scattered and have larger uncertainties. Notwithstanding this, the quadrature-phase parts of both U and V are essentially zero over the whole period range – implying that variations in the ground to pipe current are in-phase with the electric field variations. At periods between 3 and 100 minutes the in-phase part of V is about twice that of U, suggesting that I is more closely related to the electric field perpendicular to the pipeline than to the electric field parallel to it. The rise in the in-phase part of U at the longest periods, although with relatively large uncertainties, is puzzling as such long period variations are at the upper end of the period range thought to be important in producing GIC (Boteler & Pirjola, 2017). Nevertheless, it is possible that the rise in the in-phase part of U may indicate a response to the S_q variation.

A similar procedure as applied for the magnetic field transfer functions allows the orientation, ϕ, relative to the pipeline, of electric field variations that give maximum variation in I to be calculated from the equivalent expression to equation (5). Similarly, angles ϕ_{Real} and ϕ_{Imag} can be calculated from equivalent expressions to (4). In this case, the near zero values of the quadrature phase parts of U and V mean that $|Quad|$ as given by (4b) is also near-zero and, as a result, the angles ϕ_{Real} (4a) are very close to the angles ϕ shown in Table 2. In keeping with the smaller uncertainties, apart from at the shortest periods, the principal orientations, between 120 and 130° from the local pipeline orientation, are very well defined. The small uncertainties at all periods greater than 5 minutes shows the sensitivity of the variations in I to the direction of the varying electric field. The calculated orientations of 120 - 130° from the pipeline correspond to geographic directions of roughly N160 - 170°E. This is sufficiently close to being perpendicular to the local coastline that it led Ingham (1993) to hypothesis that variations in the electric field perpendicular to the coastline were instrumental in causing a varying earth potential relative to the pipeline, and that it was this that led to the observed variations in both the cathodic protection potential and the resulting ground to pipe current.

The fact that the magnetic and electric field angles θ and ϕ are not orthogonal to each other is related to the local and regional earth conductivity structure. This also results in the observed variation in angles with period, and controls the implied orientations of fields to which the current is most sensitive. Previously, Chen et al. (1990) had modeled electromagnetic induction in the New Zealand region using an analogue model. The results of this showed that the principal direction of the induced electric field is generally perpendicular to the local coastline. It was this observation, in conjunction with the directional analysis described above, that led to the hypothesis put forward by Ingham (1993) that variations in the PSP, and hence the ground to pipe current, were the result of variations in the electric field (i.e. the varying “earth” potential) perpendicular to the pipeline and coast. At the measurement site the variation in this angle slightly away from the direction perpendicular to the coastline is most likely the result of the effect of the shallowing of the resistive basement beneath the surface sediments.

The results of Chen et al. (1990) also suggested that enhancement of the telluric field perpendicular to the coastline was greatest in the region to the north of Auckland (Figure 1) where parallel coastlines are only some 10’s of kilometres apart. This in turn led to this area being deemed to have “very high” risk for variations in PSP.

4 Reanalysis

DSTL theory (Boteler, 2000; Pulkinen et al., 2001b) predicts that pipe to soil potential varies along a pipeline depending on the electric field parallel to the pipeline (E_{par}). Similarly, the current along the pipeline varies with distance and also depends upon E_{par}. The measurements shown in Figure 2 do show that the along pipe current, derivable from V_P, varies in the same manner as the ground to pipe current *I*, but is out of phase with it. The conclusions of Ingham (1993) however, based essentially, on the preceding analysis, do not fit with either the simple physical assumption of pipeline GIC being driven by variations in the magnetic field perpendicular to the pipeline, nor with DSTL theory, but instead suggest that variations in *I*, and consequently those in V_P, are not solely related to the along pipe electric field. Some further insight into resolving this contradiction can potentially be made by investigating how well the derived relationships between the ground to pipe current and the fields predict the actual observations.

4.1. System parameters

Pulkkinen et al. (2007) presented a simple method of calculating or modeling the GIC in a technological system based on an expression which relates the time series of GIC to time series of components of the electric field through system parameters *a* and *b*. In terms of the electric fields parallel and perpendicular to the pipeline, as were measured in the 1992 study, this relationship is

$$GIC(t) = aE_{par}(t) + b\,E_{perp}(t) + \epsilon(t) \qquad (6)$$

where $\epsilon(t)$ allows for the fact that all measurements have some level of noise associated with them. On the basis that the noise can be considered random and to average to zero, and is not correlated with the electric field, *a* and *b* can be calculated from

$$a = \frac{\langle GIC\, E_y\rangle\langle E_x\, E_y\rangle - \langle GIC\, E_x\rangle\langle E_y^2\rangle}{\langle E_x\, E_y\rangle^2 - \langle E_x^2\rangle\langle E_y^2\rangle} \qquad (7)$$

$$b = \frac{\langle GIC\, E_x\rangle\langle E_x\, E_y\rangle - \langle GIC\, E_y\rangle\langle E_x^2\rangle}{\langle E_x\, E_y\rangle^2 - \langle E_x^2\rangle\langle E_y^2\rangle} \qquad (8)$$

in which < . > represents an expectation value calculated from over one or more sections of data, and the x- and y-axes correspond to directions parallel and perpendicular to the pipeline. Although these relationships are based on the assumption that the time series are stationary, in general they give values of the system parameters that predict measured values of the GIC very well. For the data from the 1992 study system parameters have been calculated both for the relationship between the ground to pipe current and the measured electric fields, and also for that between the measured pipe to soil potential and the electric fields. The time series used was the 6 day period from 29 February – 05 March1992. Over this period there were considerable linear drifts in E_{par} and E_{perp}. Before calculation these drifts were removed from the data using linear fits to the measurements. *I* and *PSP* were also reduced to zero mean by having their average value subtracted. For this 6 day period the calculated variations in *I* and in *PSP*, compared to the actual measured values, are shown in Figure 6. The values of *a* and *b* for the ground to pipe current were *a* = 0.02689 km/Ω, *b* = -0.02597 km/Ω with a Pearson correlation coefficient between the measured and calculated values of ρ = 0.866. For the cathodic protection potential *a* = -14.65 km, *b* = 15.40 km with ρ = 0.872. Torta et al. (2017) also measured the goodness of fit of relationships such as (6) to measured data using a performance parameter *P* defined by

$$P = 1 - \frac{1}{\sigma_o}\sqrt{\frac{\sum[(o_i - \bar{o}) - (m_i - \bar{m})]^2}{N}} \qquad (9)$$

where *o* refers to observations, *m* to model values and σ_o to the standard deviation of the *N* observations. Values of *P* calculated for the ground to pipe current data and the cathodic protection potential are 0.500 and 0.510 respectively. The fact that for both *I* and *PSP* the magnitudes of *a* and *b* are similar supports the conclusion that the pipeline GIC depend on fields (electric or magnetic) both parallel and perpendicular to the pipeline.

Visually from Figure 6, the calculated variations in both *I* and *PSP* overall give a very good fit to the measurements. Nevertheless, it is clear that the degree to which the measured and calculated values agree varies with time. In particular the first 12 hours of the data section are not well fit. Perhaps more significant is the fact that the high frequency variations in both *I* and *PSP* during the magnetic storm of 1 March 1992 are not well reproduced but are significantly underfit. This is a reflection both of the fact that the time series are not stationary, in particular with regard to magnetic storm induced variations in the fields, and that in equation (6) the differing effects of different frequencies of variation on producing GIC are not distinguished.

4.2. Transfer function based prediction

One method of dealing with the differing effects of variations of different frequencies is to use the frequency dependent transfer functions *U* and *V* as a basis for prediction of GIC. Ingham et al. (2017) used such a transfer function technique to successfully predict GIC produced at an electrical substation in the South Island of New Zealand. This involved first calculating transfer functions between measured GIC and the magnetic field variations observed at a local geomagnetic observatory during geomagnetic storms. These transfer functions were then used in association with measured field variations during individual storms to predict the observed GIC. The same technique can be applied in the present case using the transfer functions between the ground to pipe current and the electric fields parallel and perpendicular to the pipeline

$$I(f) = U(f)E_{par}(f) + V(f)E_{perp}(f) \qquad (10)$$

Additionally, by setting either *U* or *V* to zero it is possible to test how well variations in the electric field in a single orientation are able to predict the observed current.

To do this a single 2048 minute (~ 34 hour) long data section encompassing the geomagnetic storm on 1 March 1992 has been used. The observed variations in E_{par} and E_{perp}

over this period have been Fourier Transformed and the previously calculated, period/frequency dependent, transfer functions U and V have then been used as in equation (10) to calculate the frequency spectrum of variations in I. Inverse Fourier Transformation of these gives the predicted current which can then be compared with the observations using both the correlation coefficient and the performance parameter P (9). Figure 7(a) shows the result of using both the transfer functions U and V in equation (10) to predict the ground to pipe current. The resulting correlation coefficient is 0.882 and P = 0.528. In contrast, if $V(f)$ is set to zero i.e. the ground to pipe current is predicted using only the electric field parallel to the pipe and the transfer function U, the result is as shown in Figure 7(b), with negative, and near zero, values of both correlation coefficient (-0.117) and performance parameter (-0.045). If $U(f)$ is set to zero and the current is predict using only the component of electric field perpendicular to the pipe, the result is as shown in Figure 7(c), with ρ = 0.865 and P = 0.494. These fits are summarized in Table 3.

The results of this clearly indicate that while the ground to pipe current is well modeled using equation (10), it also can be suitably modeled based only on variations in the electric field perpendicular to the pipeline. It cannot be so modeled solely using variations parallel to the pipeline. This supports the inference made by Ingham (1993) that potential corrosion of the pipe due to fluctuations in cathodic potential result primarily from variations in E_{perp}, not, as DSTL theory predicts, from variations in E_{par}.

5. Discussion

5.1. The effect of ground conductivity structure

Previous modeling of variations in PSP along pipelines has generally centred on two factors. The first of these is the induction of electric fields parallel to a pipeline by time variations of the magnetic field perpendicular to the pipeline. The induced electric fields then result in time varying currents in and out of the pipeline which disrupt the cathodic protection. The second factor is that changes in the pipeline structure, or indeed bends in the pipeline, can cause variations in PSP by disrupting the passage of induced currents. However, less attention has been paid to the effect of variations in the electrically conductivity structure of the Earth.

Boteler et al. (2003) and Fernberg et al. (2007) have presented the results of measurements of PSP at a series of locations along a transcontinental gas pipeline from Alberta/Saskatchewan to Quebec/Vermont. They observed large differences in the magnitude of PSP variations along a nearly 200 km length of the pipeline. Subsequent magnetotelluric (MT) measurements showed that the largest variations occurred at locations where the pipeline crossed major geological terrain boundaries and were associated with significant changes in induced electric fields caused by conductivity contrasts across these boundaries. The electric field to which these variations in PSP were attributed were thus those parallel to the pipeline. In contrast to this, the results presented above support the original conclusion of Ingham (1993) that variations in PSP at Dannevirke are associated with variations in the electric field *perpendicular*, not parallel, to the pipeline. Indeed, in the vicinity of Dannevirke the gas pipeline does not cross any major geological features but, rather, runs almost parallel to the main tectonic trend of the region and the associated faults.

The regional conductivity structure is associated with the tectonic setting in which the Pacific Plate is subducted beneath the Australian Plate at the Hikurangi Margin off the east coast of the North Island of New Zealand. As discussed by Ingham et al. (2001), who conducted a magnetotelluric transect across the North Island in the vicinity of Dannevirke, the main axial ranges of the lower North Island form the western boundary of the Hikurangi forearc – a region of marine sediments and Quaternary deposits lying inland from the accretionary prism associated with the subduction. Dannevirke itself lies to the western edge of this complex where the sediments of the forearc thin and the more electrically resistive greywacke of the main ranges comes closer to the surface. As mentioned above, Chen et al. (1990), using an analogue model which only considered the ocean/land boundary, modeled electric field variations to be largest in the orientation perpendicular to the coast. This was a result of the electrical conductivity contrast between seawater and land. Ingham et al. (2001) derived a two-dimensional model of electrical conductivity beneath their transect with the TM (transverse magnetic) mode of induction being perpendicular to the coastline. Their results show that the electric field perpendicular to the coastline is also significantly affected by the thinning of the conductive sediments and the shallowing of the resistive basement. This is illustrated in Figure 8, which is based on the original data from Ingham et al. (2001), and shows the magnitude, at three periods of variation, of the TM magnetotelluric impedance (i.e. the impedance in the orientation perpendicular to the coast) as a function of distance from the east coast. Up to 40 km from the coast low impedance values are associated with the Tertiary sediments of the accretionary prism. Similarly, from 80 km onwards values of impedance are again relatively low and are associated with the thick sediments of the Wanganui Basin which lies to the north-west of the axial ranges. Between these two areas the impedance is markedly higher at all three periods of variation, a rise which is associated with the resistive greywacke of the ranges. The location of the pipeline is marked by the arrow and occurs in a region where not only is the impedance significantly enhanced, but undergoes sharp variations with distance from the coast. It follows, therefore, that in this region temporal variations in the component of the electric field perpendicular to the coast are significantly larger than either closer to or further from the coast.

5.2. Corrosion risk

Using estimates from Campbell (1986) of the number of days per year a particular level of magnetic activity occurs, Ingham (1993), by estimating that current passed from pipe to ground for approximately 0.7% of the duration of a magnetic storm, and that storms of sufficient size occur 20-25 times per year, suggested an approximate corrosion rate of 5.6×10^{-4} mm/year.

By comparison Gummow (2002) suggests that a more general expression for corrosion rate (in mm/year) through a 1 cm diameter hole in a pipeline coating is given by

$$\frac{dw}{dt} = 31.25\, \Delta V\, F(p) F(t) \qquad (11)$$

where ΔV is the change in pipe potential, $F(p)$ is the fraction of steady-state (i.e. DC) corrosion due to an alternating current of appropriate period, and $F(t)$ is the fraction of time for which such a current exists. Based on Peabody (1979) $F(p)$ for variations with periods between 2 minutes and 1 hour is approximately 20%. $F(t)$ depends upon the intensity of the magnetic activity. For a storm of K_P ~ 5-6, such as the storm of 29 February-1 March 1992, $F(t)$ is estimated to be about 5%. Thus, assuming a required voltage variation of 1 V to overcome a minimum cathodic protection voltage of -0.85 V, equation (11) gives a corrosion rate of 0.31 mm/year, approximately 1% of that expected for a DC current, but well in excess of the value of 0.025 mm/year quoted by Gummow (2002) as the generally acceptable maximum value. Further, the expected current density through a hole in the pipeline coating also depends on several additional factors - the diameter of the hole, the ambient ground resistivity, and the typical variation period that causes the voltage change. Thus, actual rates of corrosion may well exceed this calculated value. The risk of corrosion of the pipeline due to overriding of the cathodic protection during magnetic storms is therefore not insignificant. In a worst case scenario even a corrosion rate of 10% of that of the 31.25 mm/year rate due to a DC current would cause breakdown of a typical pipeline wall thickness of 12 mm in less than 4 years.

6 Summary and concluding remarks

In this work we have reappraised the results of a much earlier study of variations in cathodic protection potential on a natural gas pipeline in New Zealand. Careful analysis allows the following conclusions to be drawn:

(1) Contrary to DSTL theory, in this location variations in cathodic protection potential, and measured current through an installed defect on the pipeline, are most closely related to variations in the telluric field perpendicular to the pipeline.

(2) This orientation is close to perpendicular to both the local coastline of the North Island of New Zealand and to the principal changes in earth conductivity structure associated with the tectonic setting.

(3) Both earlier analogue modeling and magnetotelluric measurements confirm that this orientation corresponds to that in which telluric fields have the largest fluctuations.

(4) It is therefore concluded that observed variations in the cathodic protection potential arise because of changes in the local potential of the ground.

(5) The risk that such variations pose to pipelines are thus affected by the regional Earth conductivity structure and does not simply arise where pipelines cross major conductivity boundaries.

(6) In this setting, at least, corrosion rates due to such variations may well approach 1 mm/year, and, in locations where variations in electric fields are further enhanced by proximity to coastlines, may be significantly higher.

Despite the results of this study apparently being at variance with the predictions of DSTL theory it remains unclear if they are widely applicable. The work of Boteler et al. (2003) and Fernberg et al. (2007) has already shown that regional electrical conductivity structure can effect pipe to soil potentials where pipelines cross major conductivity boundaries. Such boundaries can result in significant variations in the amplitudes of surface electric fields, and this is particularly true where a pipeline crosses highly resistive terrain. The import of the present study is that pipelines which are parallel and close to, but do not cross, major conductivity boundary can also experience enhanced surface electric field variations which result in large variations in pipe to soil potential. Situations where this occurs may well be restricted to locations where either pipelines run parallel to coastlines, and deep ocean water forms a major conductivity contrast with highly resistive land, or, as in the present case, where highly conductive sediments abut much more resistive terrain. Although incorporation of such effects into DSTL theory is not straight forward, such incidences are likely to be highly localized.

Acknowledgements

This research was supported by the New Zealand Ministry of Business, Innovation and Employment Hazards and Infrastructure Research Fund contract UOOX1502. Initial measurements at Dannevirke were funded by the then Natural Gas Corporation of New Zealand Ltd. We are appreciative for the efforts of Peter Simpson and Simon Harvey, IT support at Otago's Physics Department, for recovering the data reported in this study from a set of 5.25" floppy disks. Thanks to their efforts a subset of the original data remains available and is included in the supplementary material in the form of an Excel file (Dannevirke data.xlsx)..

References

Beanland, S, & Haines, J. (1998). The kinematics of active deformation in the North Island, New Zealand, determined from geological strain rates. *New Zealand Journal of Geology & Geophysics, 41*, 311-323.

Beggan, C.D., Beamish, D., Richards, A., Kelly, G.S. & Thomson, A.W.P. (2013), Prediction of extreme geomagnetically induced currents in the UK high-voltage network. *Space Weather, 11*, 407-419. https:/doi.org/10.1002/swe.200065.

Blake, S. P., Gallagher, P.T., McCauley, J., Jones, A. G., Hogg, C., Campanyà, J., Beggan, C. D., Thomson, A. W. P., Kelly, G. S., & Bell, D. (2016), Geomagnetically induced currents in the Irish power network during geomagnetic storms. *Space Weather, 14*, 1–19. https:/doi.org/10.1002/2016SW001534.

Bonner, L.R. & Schultz, A. (2017), Rapid predictions of electric fields associated with geomagnetically induced currents in the presence of three-dimensional ground structure: Projection of remote magnetic observatory data through magnetotelluric impedance tensors. *Space Weather*, *15*, 204-227. https:/doi.org/10.1002/2016SW001535, 2016SW001535.

Boteler, D.H. (2000), Geomagnetic effects on the pipe to soil potentials of a continental pipeline. *Advances in Space Research*, *26*, 15-20.

Boteler, D.H. (2013), A new versatile method for modelling geomagnetic induction in pipelines. *Geophysical Journal International*, *193*, 98-109. https:/doi.org/10.1093/gji/ggs113.

Boteler, D.H. & Pirjola, R.J. (2017), Modeling geomagnetically induced currents. *Space Weather*, 15, 258-276. https:/doi.org/10.1002/2016sw001499.

Boteler, D.H., Trichtchenko, L. & Samson, C. (2003), Investigation of earth conductivity influence on pipe to soil potentials. Proceedings, NACE Northern Region, Eastern Conference, Ottawa, Sept 15-17, 2003.

Campbell, W. H. (1978), Induction of auroral zone electric currents within the Alaskan Pipeline. *Pure and Applied Geophysics*, *116*, 1143–1173.

Campbell, W. H. (1980), Observation of electric currents in the Alaskan oil pipeline resulting from auroral electrojet current sources. *Geophysical Journal of the Royal Astronomical Society*, *61*, 437–449.

Campbell, W.H. (1986), An interpretation of induced electric currents in long pipelines caused by natural geomagnetic sources of the upper atmosphere. *Surveys in Geophysics*, *8*, 239-259.

Chen, J., Dosso, H.W. & Ingham, M. (1990), Electromagnetic induction in New Zealand: analogue model and field results. *Physics of the Earth and Planetary Interiors, 62*, 257-270.

Divett, T., Ingham, M., Beggan, C., Richardson, G., Rodger, C.J., Thomson, A.W.P. & Dalzell, M. (2017), Modeling geo-electric fields around New Zealand to explore geomagnetically induced current (GIC) in the South Island's electrical transmission network, *Space Weather, 15,* 1396-1412. https:/doi.org/10.1002/2017SW001697.

Divett T., G.S. Richardson, C.D Beggan, C.J. Rodger, D.H Boteler, M. Ingham, D.H. MacManus, A.WP Thomson, & M. Dalzell (2018), Transformer - level modeling of Geomagnetically Induced Currents in New Zealand's South Island, *Space Weather*, 16. https://doi.org/10.1029/2018SW001814.

Fernberg, P.A., Samson, C., Boteler, D., Trichtenko, L. & Larocca, P. (2007), Earth conductivity structures and their effects on geomagnetic induction in pipelines. *Annales Geophysicae*, *25*, 207-218.

Gaunt, C. T., & Coetzee, G. (2007), Transformer Failures in Regions Incorrectly Considered to have Low GIC-Risk, in IEEE Lausanne, p. 807, IEEE, Lausanne.

Gideon, D. N (1971), Telluric current effects on buried pipelines. *Materials Protection and Performance*, *10*, 5-10.

Gummow, R.A. (2002), GIC effects on pipeline corrosion and corrosion control systems. *Journal of Atmospheric and Solar-Terrestrial Physics*, *64*, 1755-1764.

Ingham, M. (1993), Analysis of variations in cathodic protection potential and corrosion risk on the natural gas pipeline at Dannevirke. Contract Report for the Natural Gas Corporation, January 1993, pp 94.

Ingham, M., Whaler, K. & McKnight, D. (2001), Magnetotelluric sounding of the Hikurangi Margin, New Zealand. *Geophysical Journal International*, *144*, 343-355.

Ingham, M., Rodger, C.J., Divett, T., Dalzell, M. & Petersen, T. (2017), Assessment of GIC based on transfer function analysis, *Space Weather*, *15*, 1615-1627. https:/doi.org/10.1002/2017SW001707.

Liu, C.-M., Liu, L.-G., Pirjola, R. & Wang, Z.-Z. (2009), Calculation of geomagnetically induced currents in mid- to low-latitude power grids based on the plane wave method: A preliminary case study. *Space Weather*, *7*, S04005. https:/doi.org/10.1029/2008SW000439.

Mac Manus, D.H., Rodger, C.J., Dalzell, M., Thomson, A.W.P.,Clilverd, M.A., Petersen, T., Wolf, M.M., Thomson, N.R. & Divett, T. (2017), Long-term geomagnetically induced current observations in New Zealand: Earth return corrections and geomagnetic field driver. *Space Weather*, *15*, 1020-1038. https:/doi.org/10.1029/2017SW001635.

Marshall, R.A., Gorniak, H., Van Der Walt, T., Waters, C.L., Sciffer, M.D., Miller, M., Dalzell, M., Daly, T., Pouferis, G., Hesse, G. & Wilkinson, P. (2013), Observations of geomagnetically induced currents in the Australian power network, *Space Weather*, *11* (*1*), 6–16. https:/doi.org/10.1029/2012SW000849.

Marshall, R.A., Waters, C.L. & Sciffer, .D. (2010), Spectral analysis of pipe to soil potentials with variations of the Earth's magnetic field in the Australian region. *Space Weather*, *8*, S05002. https:/doi.org/10.1029/2009SW000553.

Osella, A., Favetto, A. & Lopez, E. (1998), Currents induced by geomagnetic storms on buried pipelines as a cause of corrosion. *Journal of Applied Geophysics, 38*, 219-233.

Peabody, A.W. (1979), Corrosion aspects of arctic pipelines. *Materials Performance, 30*, 27-32.

Pulkkinen, A., Viljanen, A., Pajunpää, K. & Pirjola, A. (2001a), Recordings and occurrence of geomagnetically induced currents in the Finnish natural gas pipeline network. *Journal of Applied Geophysics*, *48*, 219-231.

Pulkkinen, A., Pirjola, A., Boteler, D., Viljanen, A., & Yegorov, I. (2001b), Modelling of space weather effects on pipelines. *Journal of Applied Geophysics*, *48*, 233-256.

Pulkkinen, A., Pirjola, R. & Viljanen, A. (2007). Determination of ground conductivity and system parameters for optimal modeling of geomagnetically induced current flow in technological systems. *Earth Planets and Space, 59*, 999-1006. https:/doi.org/10.1186/BF03352040.

Ritter, O. (2007). Induction arrows. In: Encyclopedia of Geomagnetism and Paleomagnetism, Editors Gubbins, D. & Herrero-Bervera, E., published by Springer, Dordrecht.

Rodger, C.J., Mac Manus, D.H.,Dalzell, M., Thomson, A.W.P., Clarke, E., Petersen, T., , Clilverd, M.A. & Divett, T. (2017), Long-term geomagnetically induced current observations from New Zealand: peak current estimates for extreme geomagnetic storms. *Space Weather, 15*, 1447–1460. https:/doi.org/10.1029/2017SW001691.

Torta, J. M., Serrano, L., Regué, J. R., Sánchez, A. M., & Roldán, E. (2012), Geomagnetically induced currents in a power grid of northeastern Spain. *Space Weather*, *10*, 1–11. https:/doi.org/10.1029/2012SW000793.

Torta, J. M., Marsal, S. & Quintana, M. (2014), Assessing the hazard from geomagnetically induced currents to the entire high-voltage power networdk in Spain. *Earth Planets and Space*, 66, 1-17. https:/doi.org/10.1186/1880-5981-66-87.

Torta, J. M., Marcuello, A., Campanyà, J., Marsal, S., Queralt, P. & Ledo, J. (2017), Improving the modeling of geomagnetically induced currents in Spain. *Space Weather*, *15*, 691-703. https:/doi.org/10.1002/2017SW001628.

Trivedi, N. B., Vitorello, C., Kabata, W., Dutra, S. L. G., Padilha, A. L., Mauricio, S. B., De Padua, M. B., Soares, A. P., Luz, G. S., De A. Pinto, F., Pirjola, R. & Viljanen, A. (2007), Geomagnetically induced currents in an electric power transmission system at low latitudes in Brazil: A case study,. *Space Weather*, *5,* S04004. https:/doi.org/10.1029/2006SW000282.

Viljanen, A. (1989), Geomagnetically induced currents in the Finnish natural gas pipeline. *Geophysica, 25*, 135-159.

Viljanen, A., Pulkkinen, A., Pirjola, R., Pajunpää, K., Posio, P. & Koistinen, A. (2006), Recordings of geomagnetically induced currents and a nowcasting service of the Finnish natural gas pipeline system. *Space Weather*, *4*, S10004, https:/doi.org/10.1029/2006SW000234.

Period (min)	**θ (°)**	**Amplitude (mA)**	**Period (min)**	**θ (°)**	**Amplitude (mA)**
2.1	-33 ± 168	0.09	52.7	-29 ± 11	0.49
3.3	45 ± 36	0.47	83.5	-29 ± 9	0.39
5.3	42 ± 76	0.54	132.4	-38 ± 11	0.24
8.4	49 ± 80	0.58	209.8	-45 ± 9	0.22
13.2	12 ± 18	0.53	332.6	-35 ± 12	0.15
21.0	5 ± 34	0.49	527.1	-19 ± 25	0.09
33.3	-21 ± 21	0.58			

Table 1: Orientation (clockwise from N39°E – the pipeline orientation) of a 10 nT variation in horizontal magnetic field which produces the given maximum variation in ground to pipe current, *I*.

Period (min)	**ϕ (°)**	**Amplitude (mA)**	**Period (min)**	**ϕ (°)**	**Amplitude (mA)**
2.1	149 ± 31	0.15	52.7	129 ± 3	0.42
3.3	54 ± 203	0.17	83.5	126 ± 3	0.41
5.3	114 ± 7	0.30	132.4	132 ± 2	0.43
8.4	122 ± 7	0.36	209.8	143 ± 7	0.52
13.2	123 ± 4	0.41	332.6	146 ± 4	0.56
21.0	119 ± 1	0.39	527.1	150 ± 6	0.63
33.3	125 ± 1	0.42			

Table 2: Orientation (clockwise from N39°E – the pipeline orientation) of a 10 mV/km variation in horizontal electric field which produces the given maximum variation in ground to pipe current, *I*.

Fit using	**ρ**	**P**
Variations in E_{par} and E_{perp}	0.882	0.528
Variations in E_{par} only	-0.117	-0.045
Variations in E_{perp} only	0.865	0.494

Table 3: Correlation coefficient (ρ) and performance parameter (P) for three different fits to the ground to pipe current based on transfer functions between *I* and electric fields parallel and perpendicular to the pipeline.

Figure captions.

Figure 1: (a) Map of the North Island, New Zealand showing the Marsden Point to Wiri pipeline, which ruptured at Ruakaka on 14 September 2017, and the pipeline at Dannevirke which is the subject of this study. (b) Detail of the layout of measurements at Dannevirke. The pipeline is shown by the dashed line, the filled square shows the location of the magnetometer, dots the locations of electrodes used to measure the telluric fields, the star the location of measurement of the cathodic protection potential, and the open square the location of the coupon through which the ground to pipe current was measured.

Figure 2: Measured variations in *H*, *D*, *N* and *E* on 1 March 1992 local time.

Figure 2 (continued): Measured variations in *PSP*, *I* and V_P on 1 March 1992 local time.

Figure 3: Variations in ground to pipe current *I* and rates of change of the horizontal magnetic field parallel (dH_{par}/dt) and perpendicular (dH_{perp}/dt) to the pipeline over a 4 hour period on 1 March 1992 local time.

Figure 4: Transfer functions *R* and *S* relating the ground to pipe current to variations in the horizontal components of the magnetic field parallel and perpendicular to the pipeline. Uncertainties are shown by error bars.

Figure 5: Transfer functions *U* and *V* relating the ground to pipe current to variations in the electric field parallel and perpendicular to the pipeline. Uncertainties are shown by the error bars.

Figure 6: Measured (green) and calculated (black) ground to pipe current and cathodic protection potential for the period 29 February – 5 March 1992 local time. Calculated values are based on equation (6) with system parameters calculated from equations (7) and (8).

Figure 7: Measured (green) and calculated (black) ground to pipe current for a 2048 minute period over 29 February – 2 March 1992. Calculated values are based on equation (10) allowing for (a) electric fields both parallel and perpendicular to the pipeline, (b) only an electric field parallel to the pipeline, and (c) only an electric field perpendicular to the pipeline.

Figure 8: Magnitude, at three different periods of variation, of the component of magnetotelluric impedance tensor perpendicular to the coast as a function of distance from the coast. The arrow marks the location of the pipeline.

Figure 1.

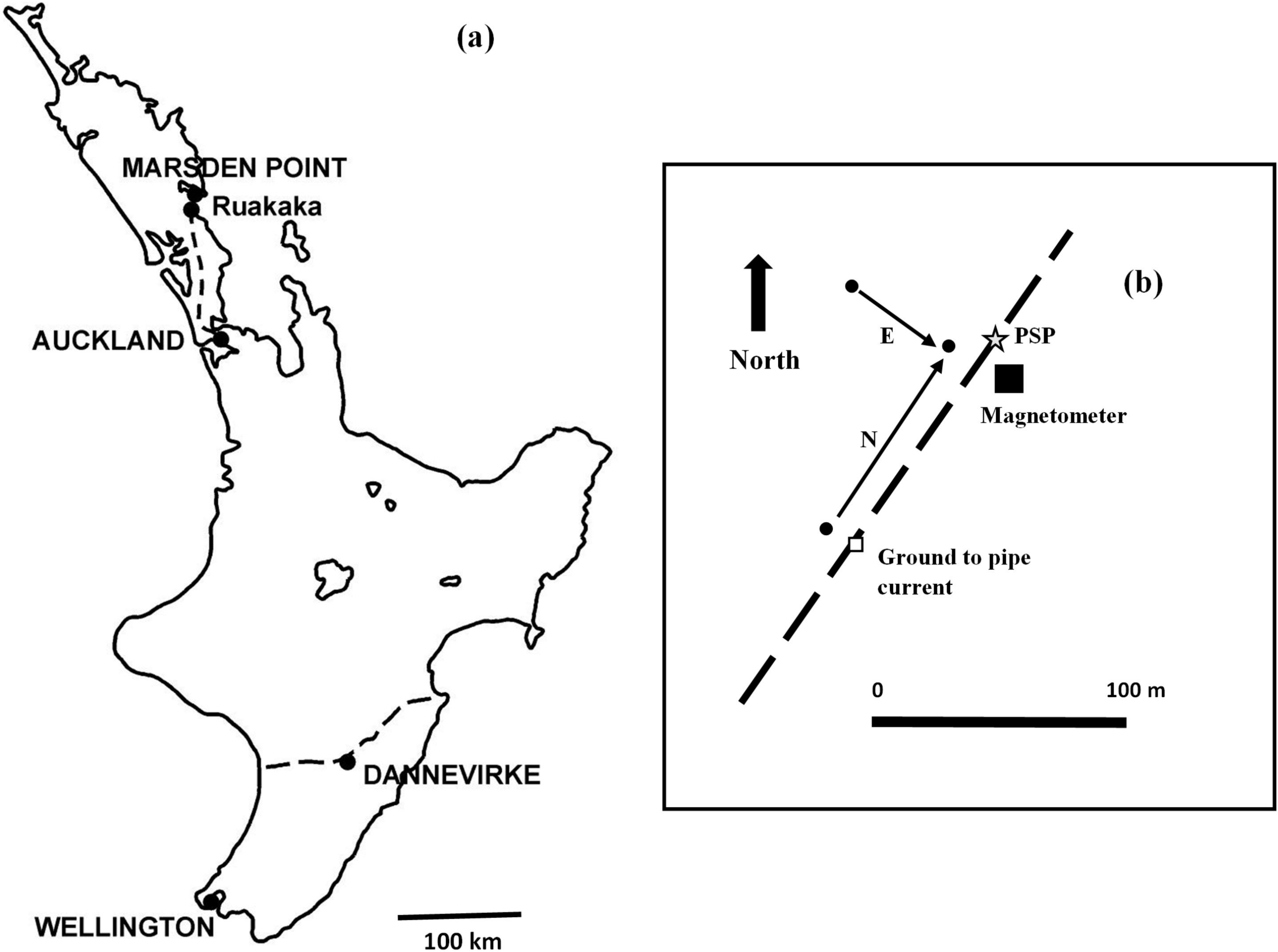
(a)
MARSDEN POINT
Ruakaka
AUCKLAND
DANNEVIRKE
WELLINGTON
100 km
(b)
North
E
N
PSP
Magnetometer
Ground to pipe current
0
100 m

Figure 2 part 1.

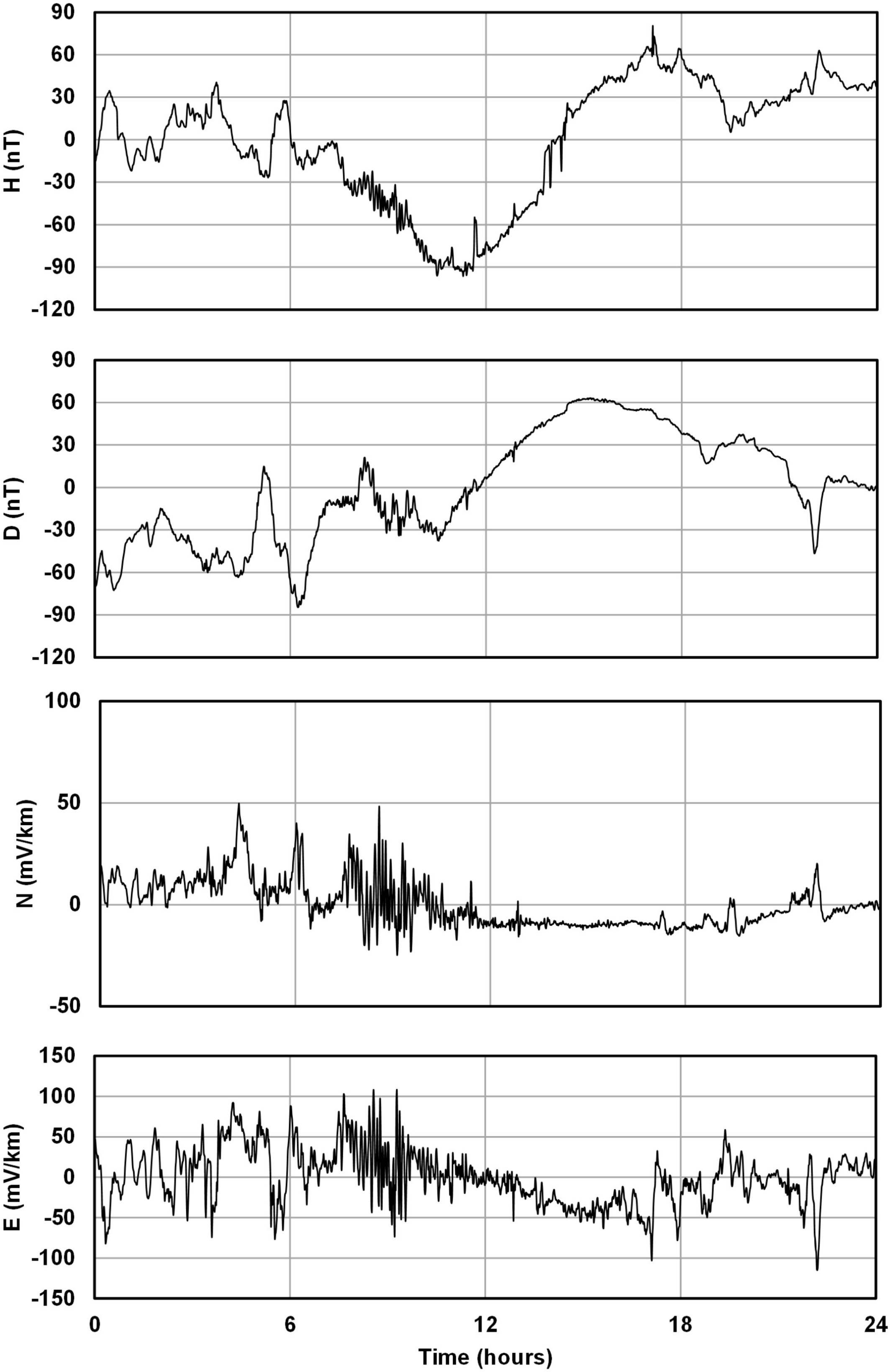
H (nT)
D (nT)
N (mV/km)
E (mV/km)
90
60
30
0
-30
-60
-90
-120
100
50
0
-50
150
100
50
0
-50
-100
-150
0
6
12
18
24
Time (hours)

Figure 2 part 2.

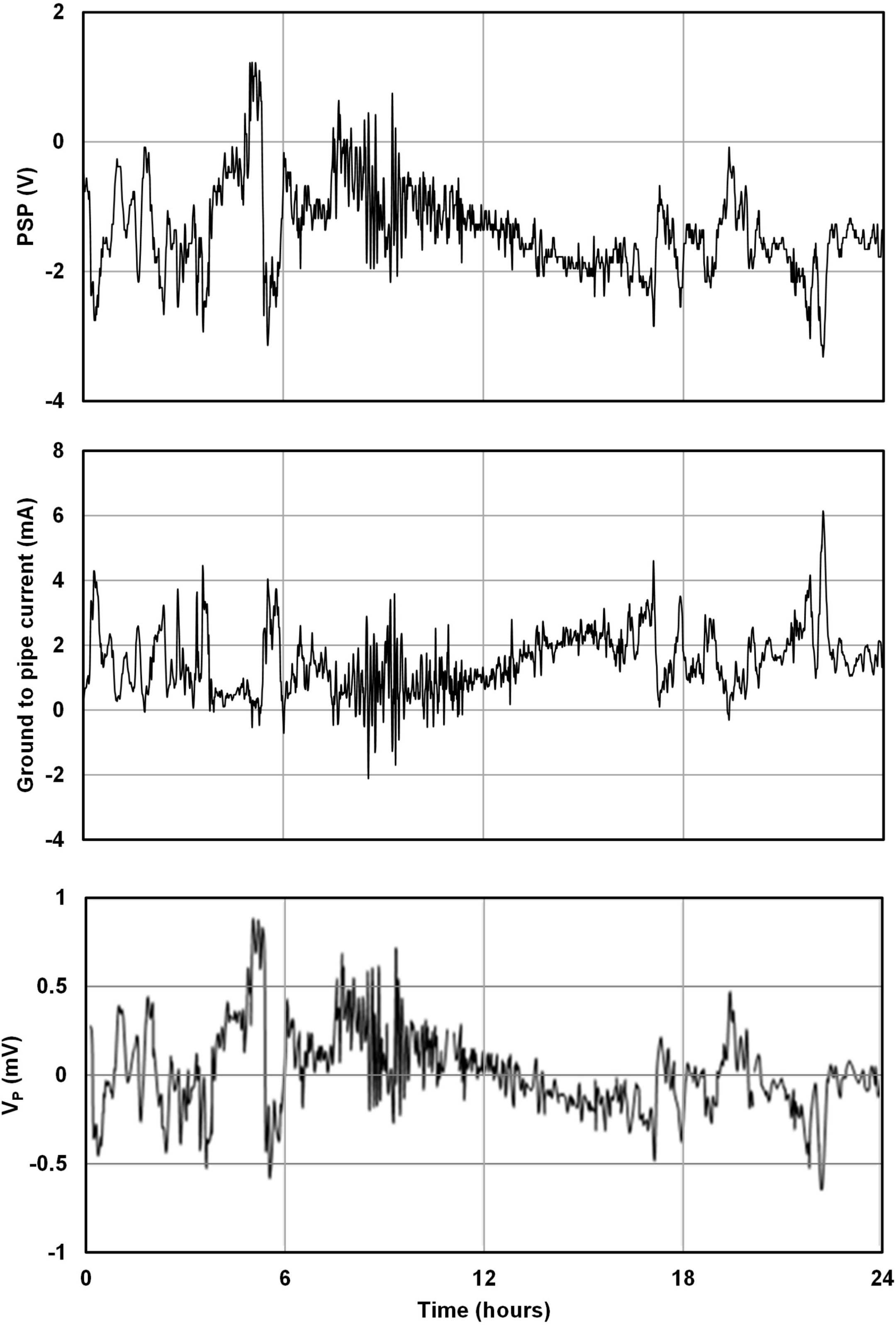

PSP (V)
2
0
-2
-4
Ground to pipe current (mA)
8
6
4
2
0
-2
-4
V_P (mV)
1
0.5
0
-0.5
-1
0
6
12
18
24
Time (hours)

Figure 3.

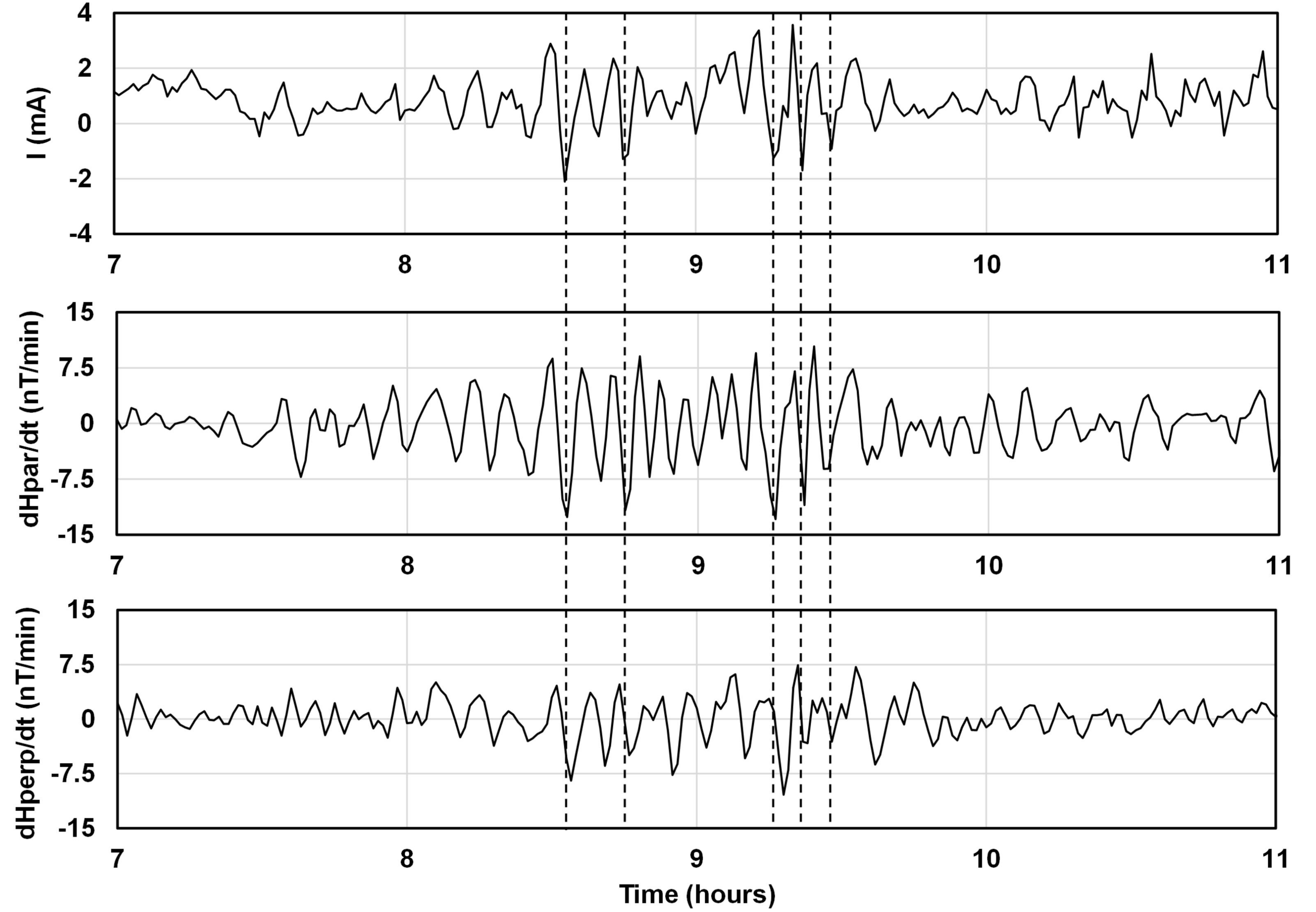

I (mA)
4
2
0
-2
-4
7
8
9
10
11
dHpar/dt (nT/min)
15
7.5
0
-7.5
-15
7
8
9
10
11
dHperp/dt (nT/min)
15
7.5
0
-7.5
-15
7
8
9
10
11
Time (hours)

Figure 4.

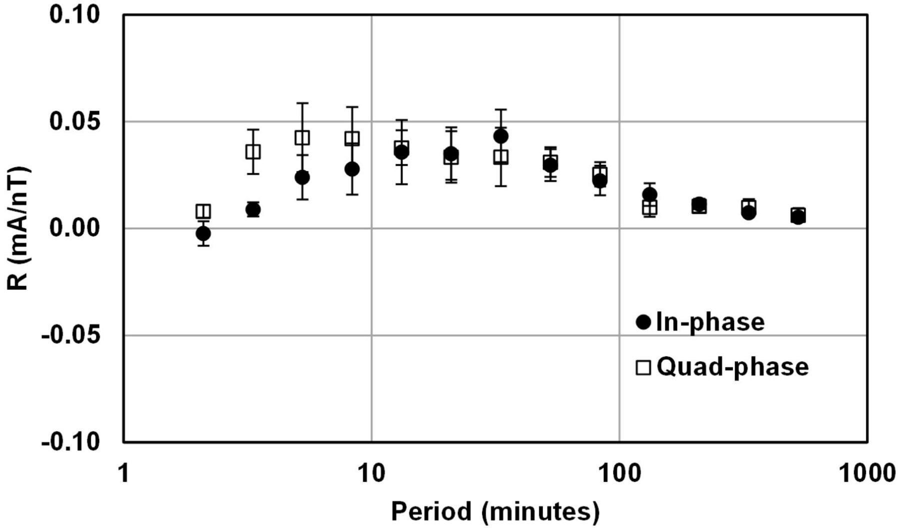
0.10
0.05
0.00
-0.05
-0.10
R (mA/nT)
In-phase
Quad-phase
1
10
100
1000
Period (minutes)

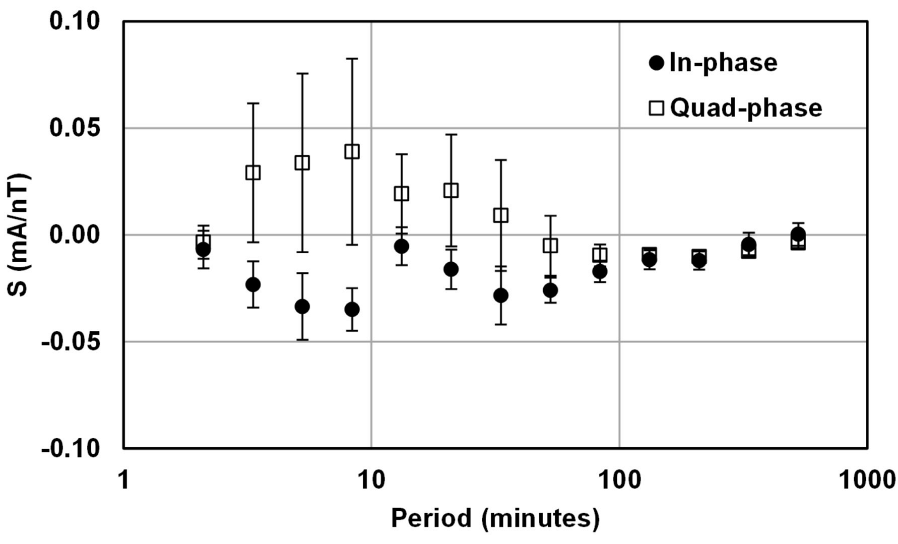
0.10
0.05
0.00
-0.05
-0.10
S (mA/nT)
In-phase
Quad-phase
1
10
100
1000
Period (minutes)

Figure 5.

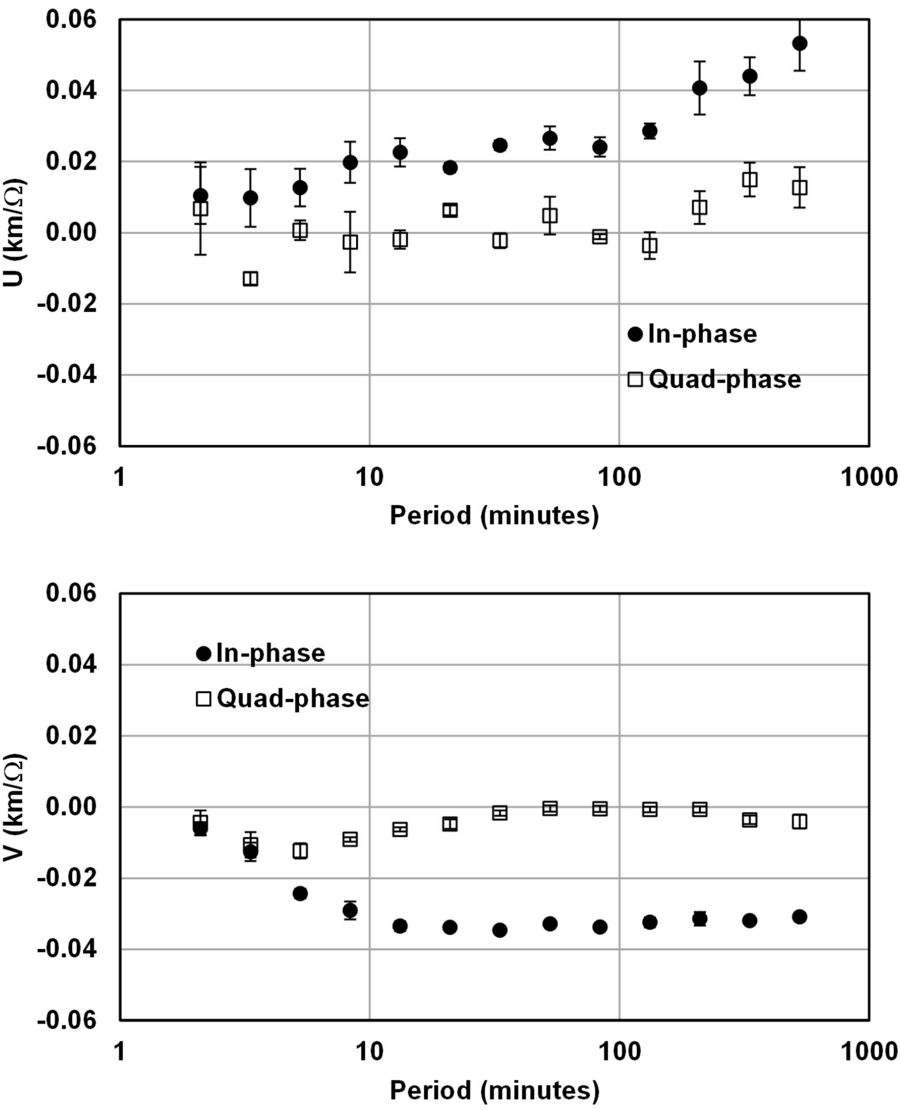

0.06
0.04
0.02
0.00
-0.02
-0.04
-0.06
U (km/Ω)
1
10
100
1000
Period (minutes)
In-phase
Quad-phase
0.06
0.04
0.02
0.00
-0.02
-0.04
-0.06
V (km/Ω)
In-phase
Quad-phase
1
10
100
1000
Period (minutes)

Figure 6.

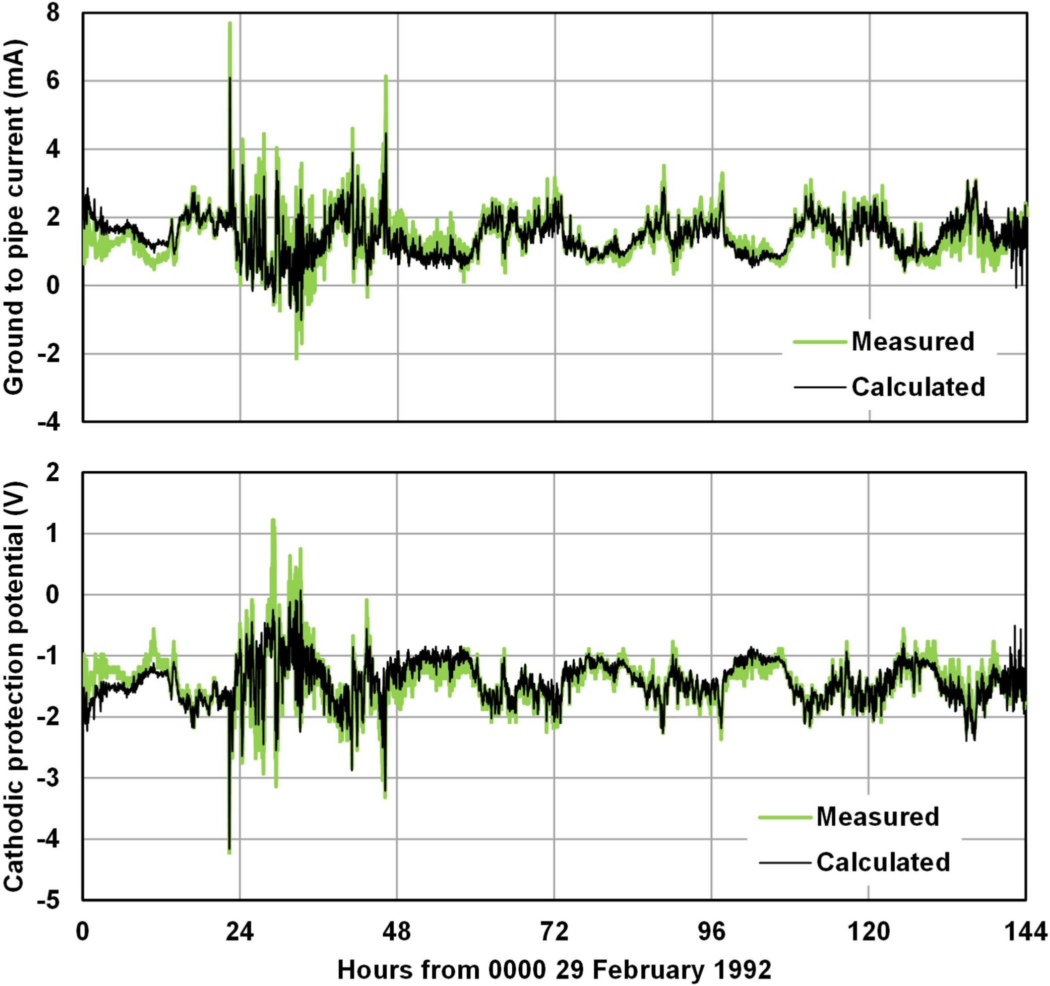

Ground to pipe current (mA)
8
6
4
2
0
-2
-4
Measured
Calculated
Cathodic protection potential (V)
2
1
0
-1
-2
-3
-4
-5
Measured
Calculated
0
24
48
72
96
120
144
Hours from 0000 29 February 1992

Figure 7.

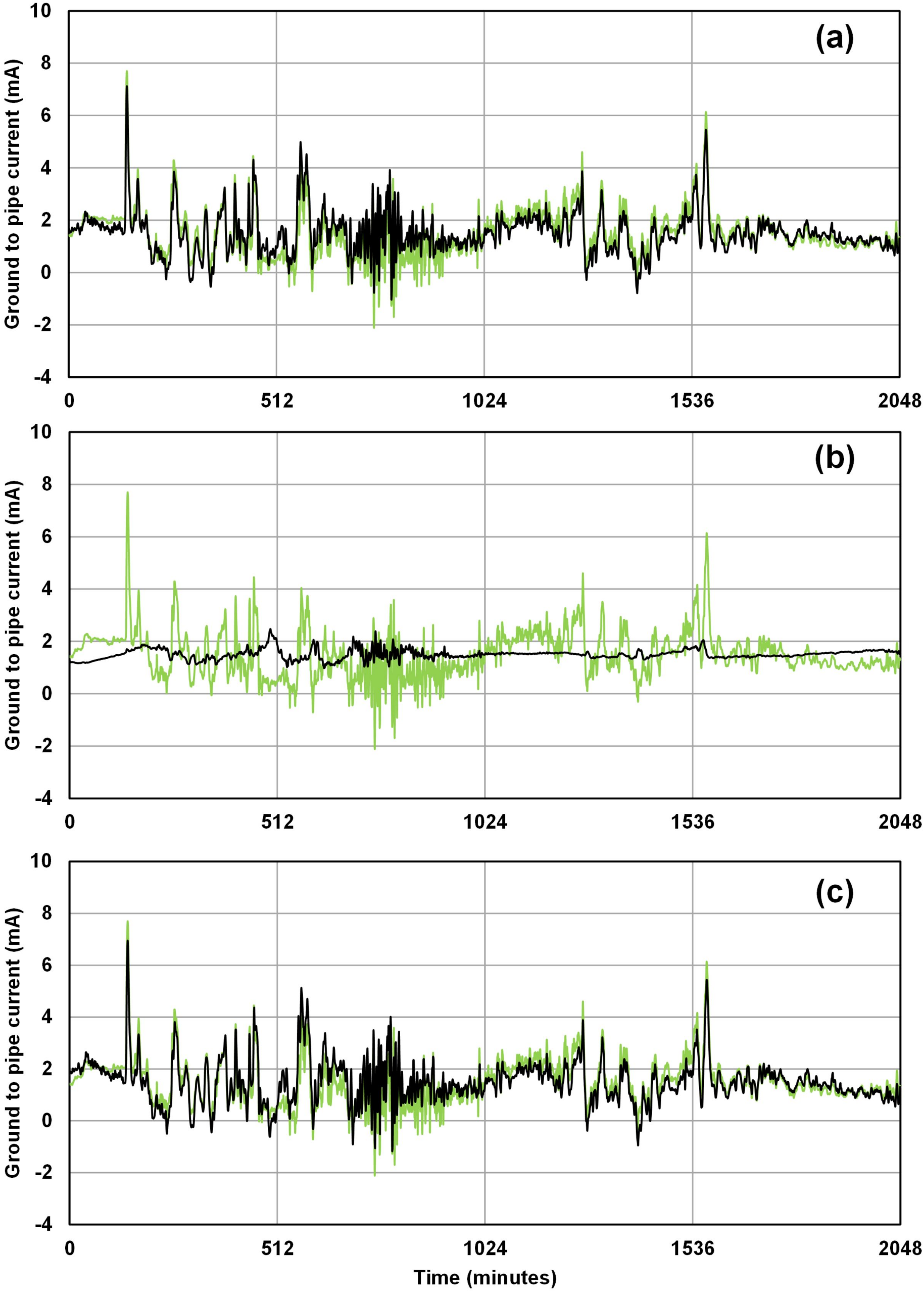
(a)
(b)
(c)
Ground to pipe current (mA)
10
8
6
4
2
0
-2
-4
0
512
1024
1536
2048
Time (minutes)

Figure 8.

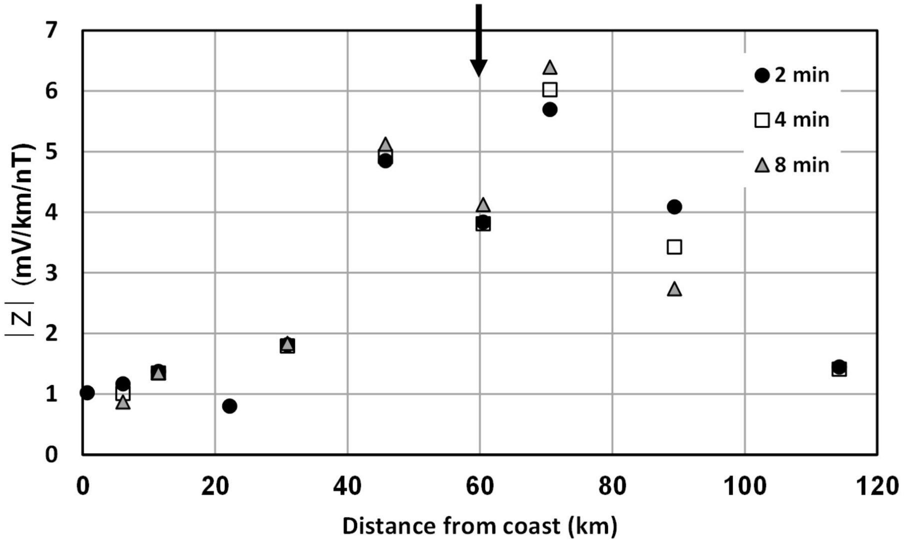

|Z| (mV/km/nT)
Distance from coast (km)
2 min
4 min
8 min
0
1
2
3
4
5
6
7
0
20
40
60
80
100
120